Structural Engineering and Mechanics, Vol. 3, No. 4 (1995) 341-358
DOI: http://dx.doi.org/10.12989/sem.1995.3.4.341

Low cycle fatigue damage assessment in steel beams

M.L. Daali †

Hatch Associates LTD., Sudbury, Ontario P3C 1X3, Canada

R.M. Korol ‡

Department of Civil Engineering and Engineering Mechanics, McMaster University, Hamilton, Ontario L8S 4L7, Canada

Abstract. The results of a series of ten W-shaped test specimens subjected to monotonic, quasi-static cyclic loading and fatigue type of loading in the form of constant amplitude tests are presented. The objectives were to assess and compare the rotation capacity and energy absorption of monotonically and cyclically loaded beams, and for the latter specimens to document the deterioration in the form of low cycle fatigue due to local buckling. In addition, strength and energy dissipation deterioration and damage models have been developed for the steel beam section under consideration. Finally, a generalized model which uses plate slenderness values and lateral slenderness is proposed for predicting rate in strength deterioration per reversal and cumulated damage after a given number of reversals.

Key words: damage; steel structures; cyclic; fatigue; deterioration; strength; energy; local buckling.

1. Introduction

The design of earthquake resistant structures requires, by necessity, allowance for some degree of damage during a seismic event in order to minimize construction cost. The minimization of cost can be achieved by providing both adequate ductility and sufficient strength so as to redistribute internal forces and thus absorb large amounts of energy.

Different modes of failure are possible in steel structures which may experience earthquake-type loading. Failure modes include excessive yielding, weld cracking, panel joint collapse, distortional buckling, local buckling, etc. Current earthquake design practice is primarily concerned with the maximum earthquake induced force or the maximum deflection that a structure might experience. Safety against total failure in moment resisting frames, for instance, is achieved through the use of design rules limiting flange and web slenderness ratios, proper weld detailing and the provision of adequate lateral supports.

Because of the randomness of the load history during an earthquake, an early high reversal of inelastic deformation might lead to initiation of local buckling in the flanges and web of a W-shaped section. Then, any secondary reversals of inelastic deformation would result in a

† P. Engineer
‡ Professor

further and continuous deterioration (in strength, stiffness and energy dissipation), which would diminish most of its useful life. Damage caused by elastic reversals in negligible; however, that caused by inelastic ones needs to be accounted for. Thus, structures designed for earthquake loading can be weakened or damaged by a combination of reversals of inelastic deformations and high deformation excursions. It seems clear, therefore, that to properly assess the rotation capacity and energy dissipation performance of W-shaped beams, damage criteria are needed that not only account for maximum response (force or displacement), but which also include the effects of repeated cyclic loadings.

This paper, then, examines the behaviour of ten specimens tested under different load histories representing monotonic, cyclic and fatigue types of loading. The experimental results of the monotonic and cyclic tests are compared to each other in order to shed some light on the effects of load history. Those of the low cycle fatigue tests are used to generate a Coffin-Manson (Tavernelli and Coffin 1961) type of plastic rotation range to strength, or energy deterioration rate per reversal relationship; in addition, earlier experimental results have been used to generate a comprehensive model that can be used in numerical simulations to assess the strength deterioration per reversal for beams subjected to earthquake-type loading.

2. Prior research in low cycle fatigue

A number of researchers recognized that failure of a structural element could result from low cycle fatigue rather than maximum response be it force or displacement. For instance, for macroscopic sized beams, Sherbourne (1963), Krishnasamy & Sherbourne (1968), Kasiraj and Yao (1969) and Gyoten, *et al.* (1974) investigated low-cycle fatigue behaviour with a view to providing insights on the behaviour of ductile structures under repeated loads; meanwhile, Neale and Schroeder (1971) considered instability under cycles of plastic deformations. On the element level, Yamada (1969) investigated experimentally the ductility-number of cycles to failure relationship for some steel and reinforced concrete beam-columns while Mizuhata, *et al.* (1977) investigated failure by crack propagation. Krawinkler, *et al.* (1983) and Krawinkler (1982, 1987) addressed the question of damage accumulation due to local buckling in steel members subjected to earthquake ground motions; they presented some guidelines for the performance assessment of structural components. More recently, Castiglioni and Goss (1989), Castiglioni (1992) and Castiglioni and Losa (1992) examined the deterioration to number of cycles relationship in steel members under cyclic loading while Calado and Azevado (1989) and Calado (1992) addressed low cycle damage modelling at the fibre level of individual members and thence its application on the structural level.

3. Experimental program

3.1. General

Two series of W-shaped beams with W310×39 and W310×21 sections having flange and web slenderness ratios, $b/2t=8.25$ and 8.85, and $h/w=48.33$ and 57.18 respectively, were selected for ten test specimens. These were fabricated as cantilever beams (Fig. 1) and are representative of a half beam length in moment resisting frames subjected to earthquake loading.

The W310×39 sections, column stub and end plates of the cantilever beams were made from

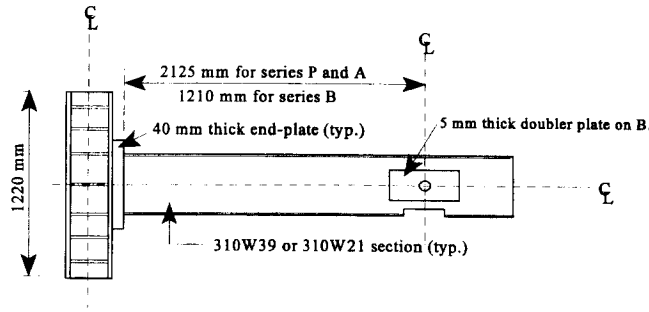

Fig. 1 A typical specimen with stub column

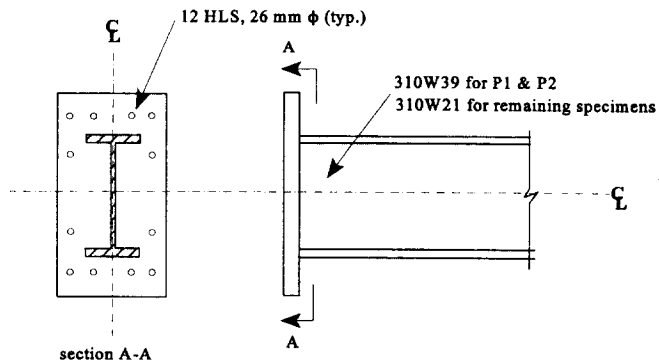

Fig. 2 Typical fabrication detail

CSA-G40.21-M-300W steel (Fy=300 MPa, Fu=450 MPa), while the W310×21 sections were of grade ASTM 36 (Fy=290 MPa, Fu=415 MPa) grade steel. The fasteners used to fix the end plates to the column stub were high strength bolts of grade ASTM A490. The end plates were welded to the W-shaped beams using E480xx electrodes and conform to the CSA W59 Standard.

The test specimens had the following characteristics: P1 and P2 were of W310×39 section and had lengths of 2125 mm, while specimens A0, A1 and A2 were of the same span but of size W310×21. Specimens B0, B1 and F1 to F3 were similar to the A-series specimens except that they had lengths of 1210 mm. The end plates were 510×310×40 mm with 26 mm diameter holes to accommodate twelve M24 A490 bolts used to connect a beam section to the column stub. Fabrication details of these specimens are shown in Fig. 2.

Specimens P1, A0 and B0 were tested under a monotonic load while P2, A1, A2 and B1 were subjected to a cyclic load history L1. The remaining three specimens, F1, F2 and F3 were tested under three different constant amplitude cycles, represented by load history L2. Fig. 3 shows typical displacement controlled load histories used in these tests.

Under earthquake motion, a structure and its members exhibit a complex response history. Rather than simulate the actual load history and its rate of loading, it has been accepted practice to assess the ability of a member to perform satisfactorily with the use of quasi-static load histories. This is done on the basis of the work by Hanson (1971) and Almuti and Hanson (1973), in which was demonstrated the validity of using quasi-static hysteresis measurements

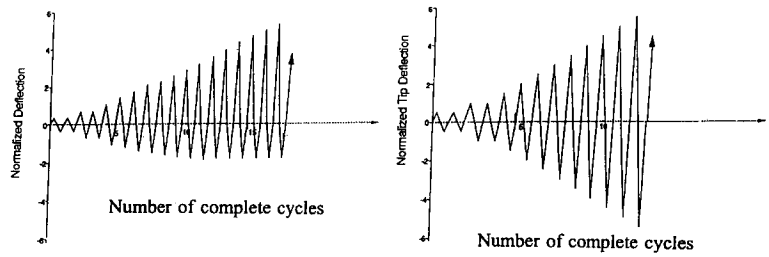

a- Non-symmetric or symmetric load history, L1

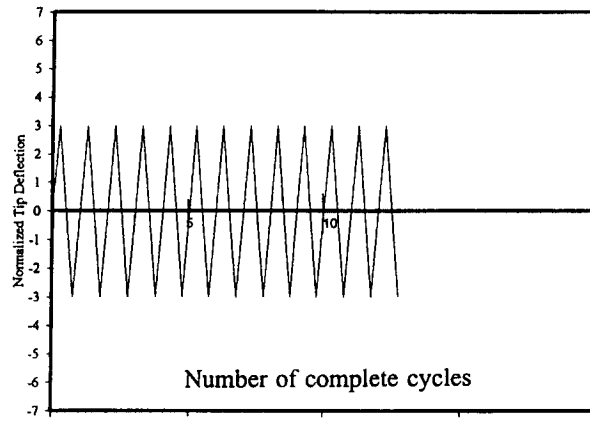

b- constant amplitude load history, L2

Fig. 3 Load histories

to predict dynamic response.

Linear Voltage Displacement Transducers (LVDT's) and strain gauges were used to monitor the response of each specimen. A load cell was used to monitor the load transferred from the hydraulic reversible acturator to the tip of the beam. The vertical deflection of the tip of the beam was measured with an LVDT, while a data acquisition system was employed with all the measuring devices. The acquired information were then passed on to a computer for storage and processing.

The experimental objective was to obtain knowledge of the restoring force characteristics of beams subjected to monotonic, cyclic and constant amplitude loading in view of rotation capacity and strength and energy deterioration per reversal of loading. This knowledge would allow for an assessment of the delivered rotation capacity of monotonically and cyclically tested specimens and an assessment of the strength and energy deterioration per reversal of loading for fatigue tested specimens.

3.2. Test results

3.2.1. Specimens P1, A0 and B0

The behaviour of this set of specimens, tested under monotonic loading, is illustrated by the

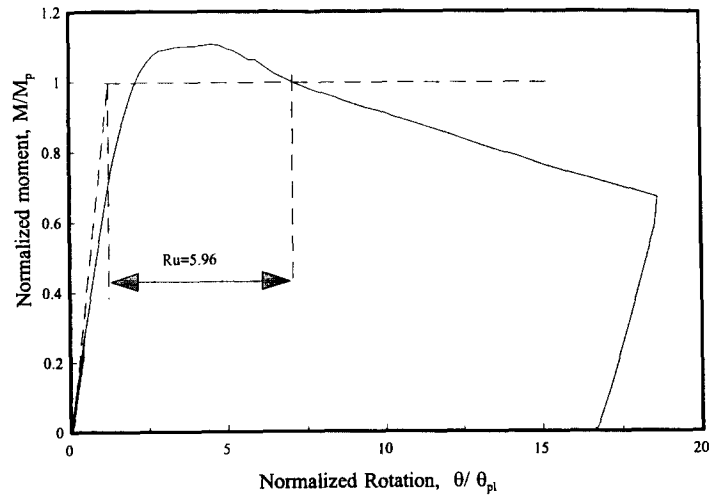

Fig. 4 Normalized moment-rotation hysteresis loops for specimen A2

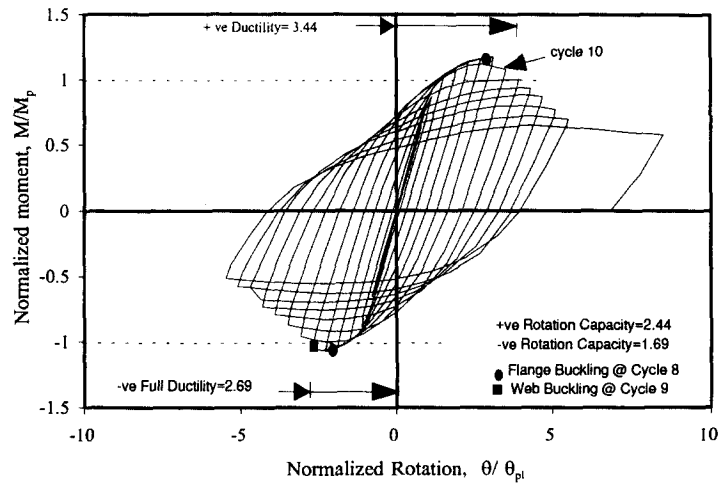

Fig. 5 Normalized moment-rotation curve for specimen B0

typical normalized moment-rotation curve of specimen B0 shown in Fig. 4. In the figure, the ratio of the maximum moment to the plastic moment M_p is plotted against the beam end rotation. In these specimens, the bending moment continued to increase until buckling was initiated in the compression flange. Indeed, the maximum response load was not reached until the onset of web buckling was observed. After reaching their maximum strength, the beam sections suffered a load fall-off eventually sustaining resisting moments equal to the nominal plastic moment values at rotation capacities of 5.88, 5.10 and 5.96 for specimens P1, A0 and B0 respectively. The tests were eventually terminated because of lateral torsional buckling occurring in the compression flange at the plastic hinge location.

3.2.2. Specimens P2, A1, A2 and B1

These specimens were selected for illustrating cyclic behaviour of beams. Typical hysteretic

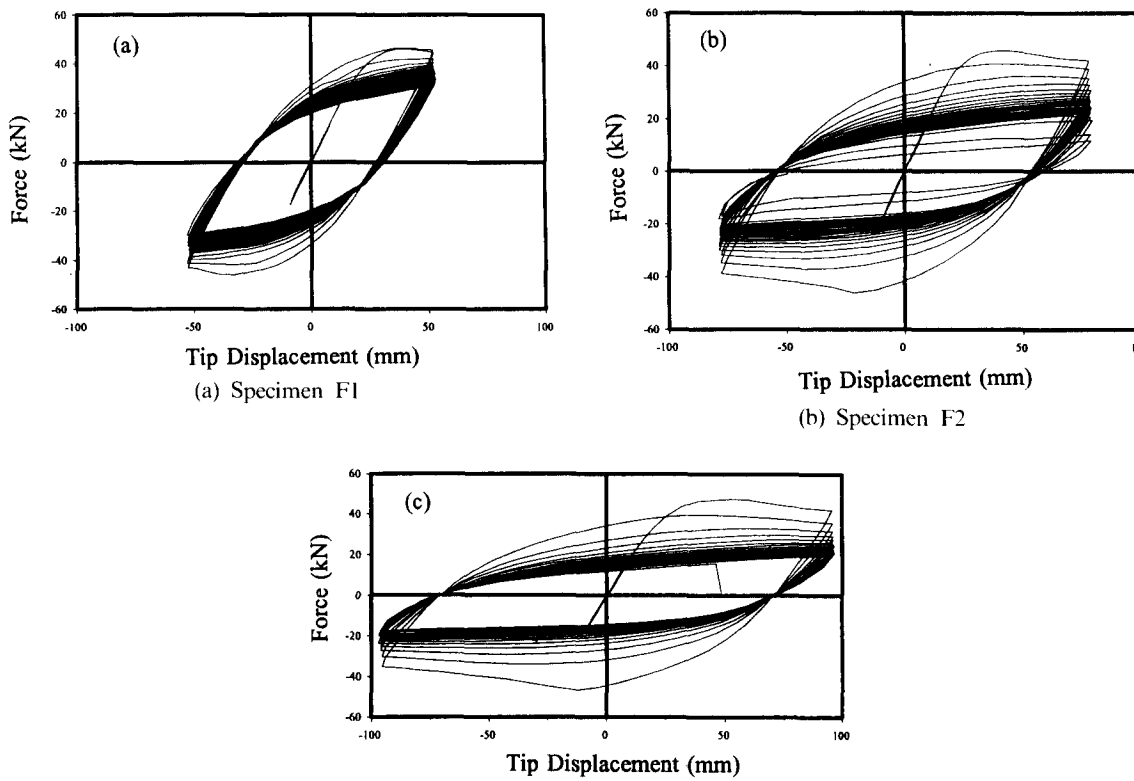

(a) Specimen F1

(b) Specimen F2

(c) Specimen F3

Fig. 6 Force displacement hysteresis loops for F-series specimens.

loops for specimen A2 are shown in Fig. 5. In the early stages of the tests, the hysteresis loops displayed stable restoring force characteristics. With additional increases in the inelastic rotations, resistance drop-offs started to occur as a consequence of flange and web buckling. Examination of Fig. 5 shows that the beginning of local flange buckling and web buckling were evident in cycles 8 and 9 as indicated by the round and square symbols. Following the local buckling of the flanges and the web, the load carrying capacity of the member started gradually degrading from one cycle to the next. In the case of specimen A2, the beam's resisting moment dropped below the plastic moment at a positive and negative rotation capacity values of 4.44 and 2.98, as measured from a zero displacement intercept. Meanwhile, specimens P2, A1 and B1 developed positive and negative rotation capacity values of (+5.75, −5.34), (+3.28, −3.7) and (+5.31, −4.81) respectively. The tests were terminated because of lateral torsional buckling occurring in the plastic hinge zone or at the stroke limit of the hydraulic actuator.

3.2.3. Specimens F1, F2 and F3

Specimens F1, F2 and F3 were tested at constant reversible amplitudes of ± 52.5, ± 79 and ± 96 mm corresponding to about 3, 4.5 and 5.5 times the plastic displacement of the respective beams. Local buckling was generally initiated in the first upward push causing the top flange to undergo compression. Immediately thereafter, local web buckling appeared at a distance equal to about the half-depth of the section. At maximum amplitude, the combined flange and web

Table 1 Summary of experimental results

Specimen # (1)	M_{max}(kN·M) (2)	M_{max}/M_p (3)	Positive rotation capacity (4) $(\theta_{max}/\theta_{pl})$-1	Negative rotation capacity (5) $(\theta_{max}/\theta_{pl})$-1
P1 (monotonic)	238.29	1.129	5.88	–
P2 (cyclic)	252.84	1.198	5.75	0.41
A0 (monotonic)	101.17	1.19	5.10	–
A1 (cyclic)	99.92	1.118	1.92	0.82
A2 (cyclic)	99.93	1.117	2.44	1.69
B0 (monotonic)	103.58	1.107	5.96	–
B1 (cyclic)	109.62	1.208	3.10	2.78

M_p is the plastic moment obtained using the tensile coupon yield stress.
M_{max} is the actual maximum moment obtained during the test.
θ_{max} is the maximum beam rotation from zero rotation intercept to the point at which M_p is exhausted.
θ_{pl} is the rotation corresponding to the actual plastic moment.

local buckling caused the specimens to undergo noticeable deterioration in strength and stiffness in the first reversal (Fig. 6). In the following few reversals, the specimens continued to sustain an appreciable rate of deterioration in strength and dissipated energy. After about 10 reversals of constant amplitude, the rate of deterioration in strength and energy dissipation slowed down. This is clearly identified by the closeness of the hysteresis loops in Fig. 6. In the last few reversals, fatigue effects led to the appearance of a crack opening in the top flange, thus leading to a subsequent increase in the rate of deterioration in strength and dissipation of energy.

4. Discussion

4.1. Comparison of monotonic and cyclic tests

The available ductility Δ_u/Δ_p and rotation capacity R_u are ductility parameters that determine how effectively internal moments can be redistributed once the plastic tip load P_p (or M_p) is reached at a given cross section. Within this context, rotation capacity is defined as the amount of total rotation, beyond the plastic limit that can be sustained before unloading below M_p takes place and is herein given by: $R_u = \frac{\theta_u}{\theta_{pl}} - 1$

Examination of Table 1 shows that specimens P1, A0 and B0, tested under monotonic loading, developed generally higher rotation capacities than did specimens P2, A1, A2 and B1 which were tested under cyclic loading. For instance, specimen A0 developed a rotation capacity of 5.1 under monotonic loading; whereas, specimens A1 and A2, similar to A0, developed maximum positive and negative rotation capacity values of (+1.92, −0.82) and (+2.44, −1.69) respectively under cyclic loading. The same trend is observed when comparing specimen P1 with P2 and specimen B0 with B1. It is clear that such differences in rotation capacity values are the result of the repeated cyclic effects which reflects a softening in member behaviour due to flange and web buckling.

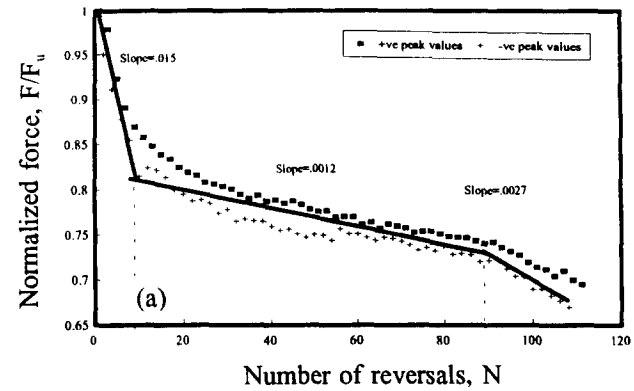

(a) Specimen F1

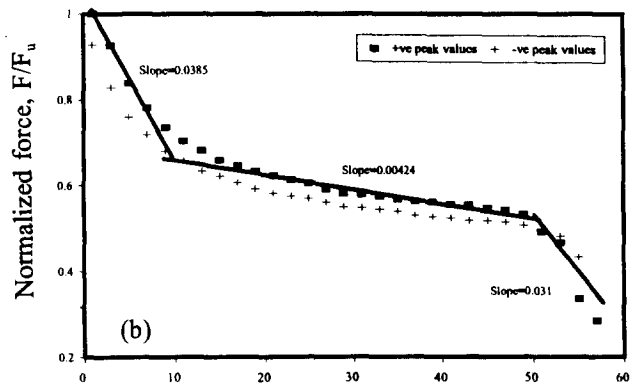

(b) Specimen F2

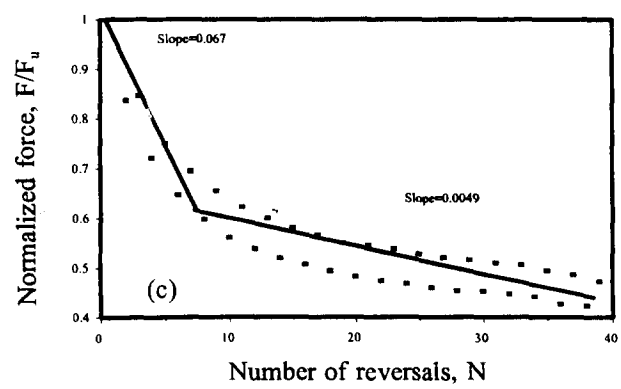

(c) Specimen F3

Fig. 7 Normalized force per reversal of loading for F-series specimens.

4.2. Constant amplitude tests

4.2.1. Rates of deterioration

Constant amplitude tests provide information on the fatigue performance parameters of sections

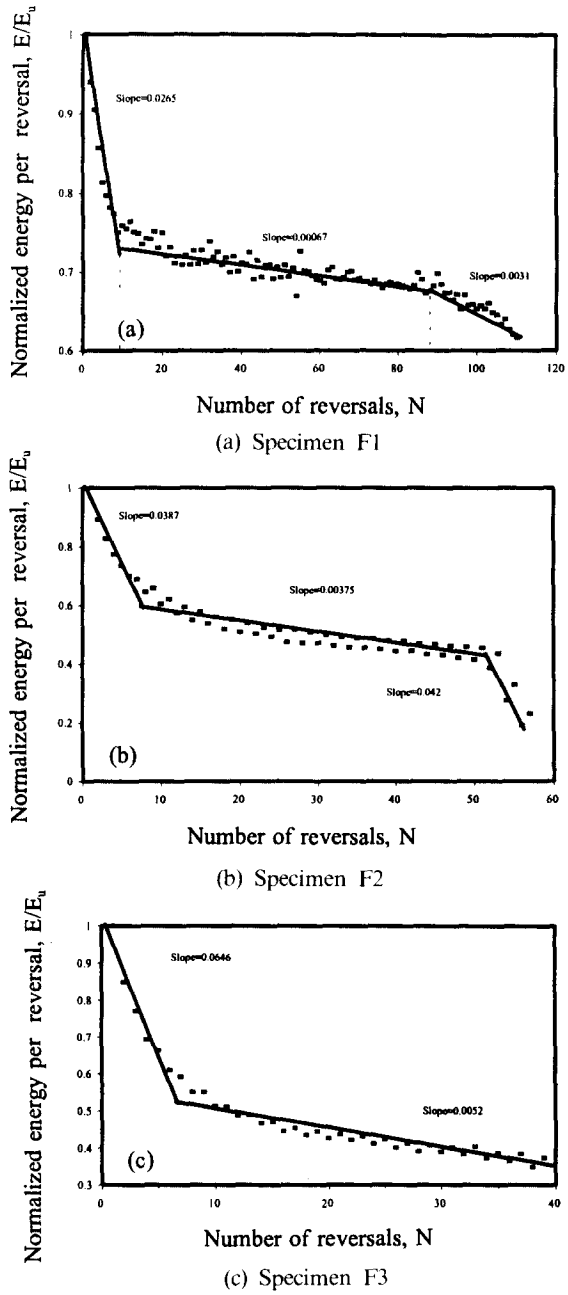

(a) Specimen F1

(b) Specimen F2

(c) Specimen F3

Fig. 8 Normalized energy per reversal of loading for F-series specimens.

under dynamic loading. Three specimens, F1 to F3, were tested at different constant amplitudes. The specimens' hysteresis loops were then used to yield information on the rates of deterioration of strength and dissipated energy. For instance, from the test results of specimen F1, the positive and negative forces F at peak displacements were normalized with respect to the ultimate force F_u reached in reversal 1. Following that, the normalized forces were plotted against the number of reversals the specimen underwent. Fig. 7(a) shows the deterioration in strength versus the number of reversals N. It is clearly seen that after undergoing a high rate of deterioration, the

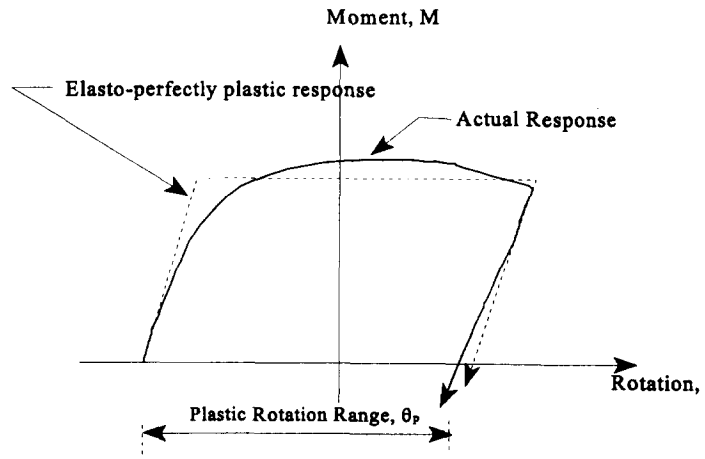

Fig. 9 Definition of plastic rotation range.

loss in strength considerably stabilized between reversals 20 to 90. Once cracking developed in the bottom flange, the specimen again showed increased deterioration. In a similar manner, the normalized energy E/E_u for specimen F1 is plotted against the number of reversals in Fig. 8. E_u is defined as the dissipated energy during the first full reversal of loading. It is clear from Fig. 8(a) that after undergoing initially high deterioration in the dissipated energy, the deterioration rate stabilized between reversals 20 to 90. Test results of specimens F2 and F3 were treated in a similar manner as those of specimen F1 and are also shown in Figs. 7 and 8. In these plots, it can be observed that at least two ranges of deterioration can be identified by their different rates of deterioration. To simplify, regression analysis was used to yield straight lines which fit the experimental results. The slopes of these lines represent the rates of deterioration per reversal for each of the ranges. For example, the strength of specimen F1 degraded in the first few reversals at a rate of 0.015 given by the slope of the line; in the following reversals, the rate of degradation of the resisting force diminished to a value of 0.0012. After that, deterioration increased again to a value of 0.0027 until failure. From the figures, one can note that the initial rate of degradation in strength and dissipated energy changed after about the first ten to fifteen reversals both in terms of loss in strength and accompanying energy. The second point of transition was less well defined for the specimens tested occurring in the range of 50 to 90 reversals.

4.2.2. Modelling of damage due to local buckling

An important parameter for measuring bending deformation in a member is the plastic rotation range θ_p experienced by a member during cyclic loading. For one event of loading, θ_p is obtained by dividing the total inelastic deformation at zero load by the member length. Fig. 9 shows a typical plot of such response in a constant amplitude test. A log-log plot of the plastic rotation range values versus the rates of deterioration values in both strength and dissipated energy is shown in Fig. 10 for each of the F-series specimens, F1 to F3, and is very suggestive of a linear pattern-type distribution. If a straight line were to be fitted to the experimental results, we obtain a Coffin-Manson type of equation (Tavernelli and Coffin 1961) of the form $\Delta d = a(\theta_p)^b$, where Δd is the deterioration per reversal and a and b are experimental parameters that reflect

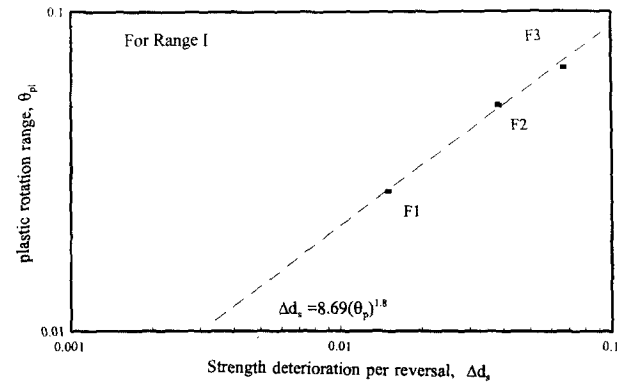

(a) Strength deterioration

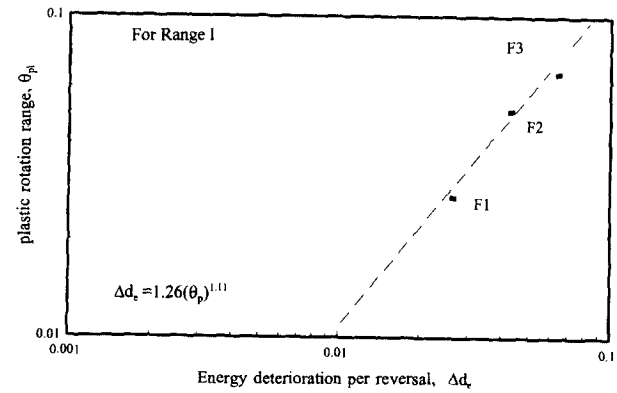

(b) Energy deterioration

Fig. 10 Strength or energy deterioration per reversal of loading for F-series specimens.

the properties of the member under a constant amplitude test. For the W310×21 section under consideration, a least square analysis of the differences of the test results and predicted results yields the following relationships for range I or in other words the first few reversals of loading;

$$\Delta d_s = 8.69(\theta_p)^{1.80} \text{ for strength deterioration per reversal} \quad (1)$$

$$\Delta d_e = 1.26(\theta_p)^{1.11} \text{ for energy deterioration per reversal} \quad (2)$$

If failure is defined by the attainment of some percentage loss in strength or energy dissipation, 10% to 20% say, then, the total number of reversals to failure for a constant amplitude test can be written as $N = 1/\Delta d$.

If Miner's rule (Miner 1945) of linear damage accumulation were used, then for variable amplitude tests the cumulated damage d after N reversals of different magnitudes θ_{pi} is given by

$$d = a\sum(\theta_{pi})^b \quad (3)$$

and $N = a^{-1}\sum(\theta_{pi})^{-b}$. Note that θ_{pi} is simply θ_p during the ith positive or negative reversal. As suggested by Krawinkler (1982), if x is introduced as a limit of damage acceptability (10-15% say), then the total number of reversal to failure is given by $N = xa^{-1}\sum(\theta_{pi})^{-b}$ and the cumulated damage is: $D = x^{-1}a\sum(\theta_{pi})^b$.

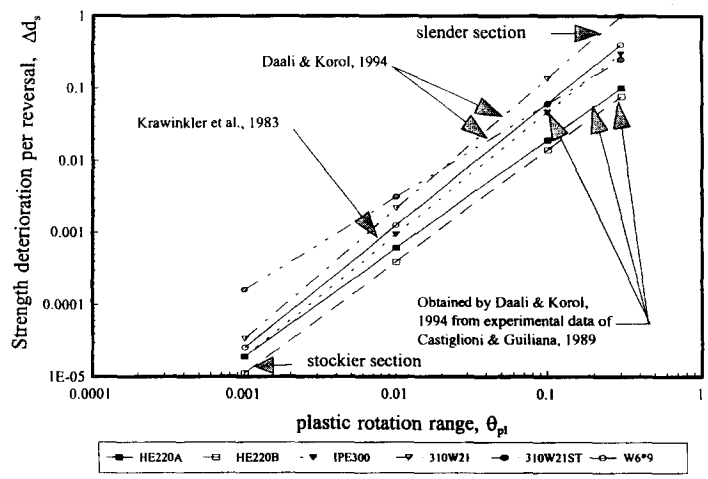

Fig. 11 Strength deterioration models for different sections.

Table 2 Observed and predicted section parameters

References	Sections	α_f	α_w	α_l	α_e	Observed		Empirically obtained	
						a	b	a	b
1	W310*21	8.85	57.71	41.88	0.711	8.69	1.81	8.19	1.648
2	W6*9	9.43	32.17	30.89	0.311	3.05	1.69	2.48	1.648
3	HE220A	10	26.8	25.59	0.228	0.61	1.5	1.28	1.648
3	HE220B	6.9	19.8	25.23	0.114	0.50	1.55	−0.33	1.648
3	IPE300	7	39.2	42.15	0.384	2.298	1.69	3.52	1.648

1: Authors
2: Krawinkler (1983)
3: By Authors from experimental data of Castiglioni and Guiliana (1989)
Note: a and b are parameters defined in Eq. 3.

4.2.3. Empirical model for damage assessment in beams

Strength deterioration models from five different sections are shown in Fig. 11. It is clearly seen that although showing a similar trend, the sections yield different strength deterioration rates per reversal of loading. Since in practice, it is common to at least indirectly select beams according to their flange slenderness, web slenderness and lateral slenderness ratios, it was decided to try to predict empirically the member parameters a and b according to these slenderness ratios.

Values of the parameters a and b from strength deterioration models are given Table 2 with their corresponding slenderness ratios. Plots of the parameters a and b versus the modified flange slenderness value $\alpha_f\left(=\frac{b}{2t}\sqrt{\frac{\sigma_y}{300}}\right)$, the modified web slenderness $\alpha_w\left(=\frac{h}{w}\sqrt{\frac{\sigma_y}{300}}\right)$ and the modified lateral slenderness $\alpha_l\left(=\frac{L}{r_y}\sqrt{\frac{\sigma_y}{300}}\right)$, where units of σ_y are in MPa, show no clear pattern; however, those of the same parameters versus the effective slenderness α_e expres-

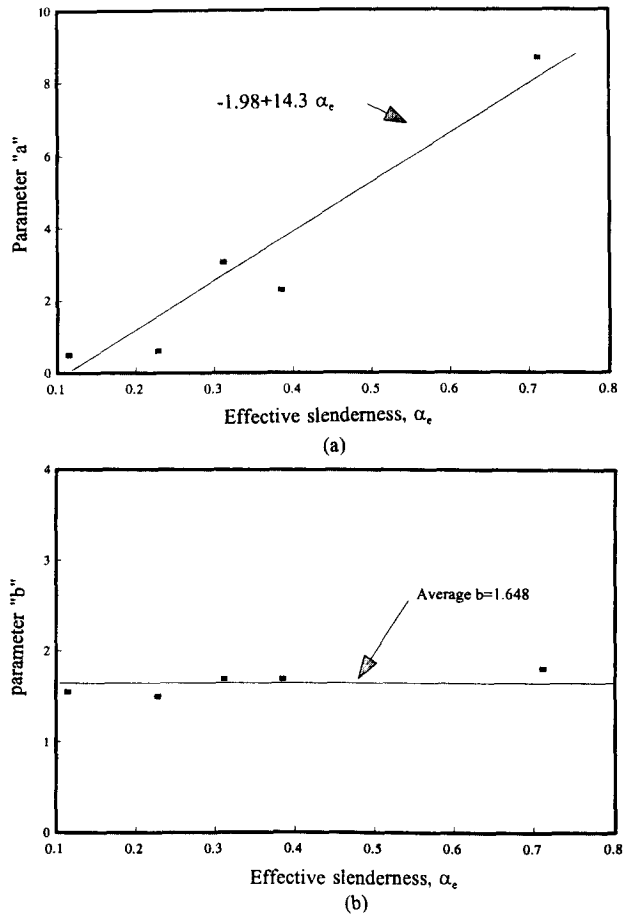

Fig. 12 Effective slenderness, α_e.

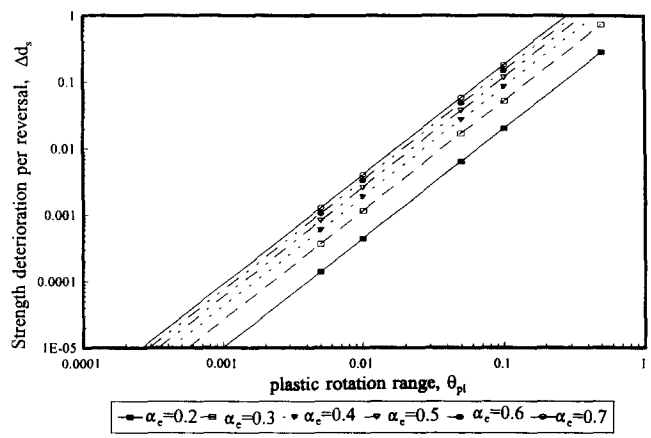

Fig. 13 Model for predicting strength deterioration in beams.

sed as a normalized product of the three above mentioned slenderness, *i.e.*, $\alpha_f \alpha_w \alpha_l$ 30072, clearly shows a trend. With increasing values of the effective slenderness α_e the values of parameter

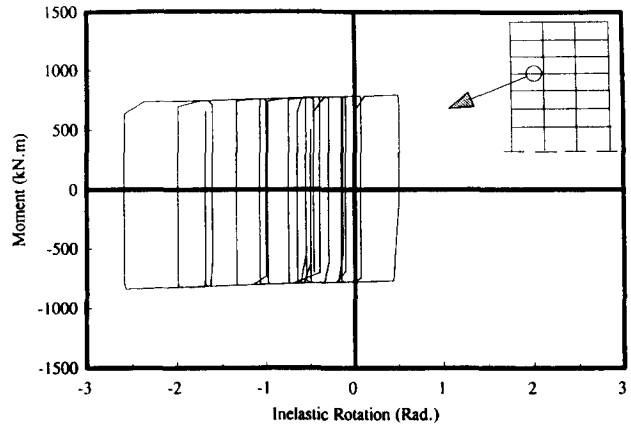

(a) Moment-inelastic rotation response in a beam

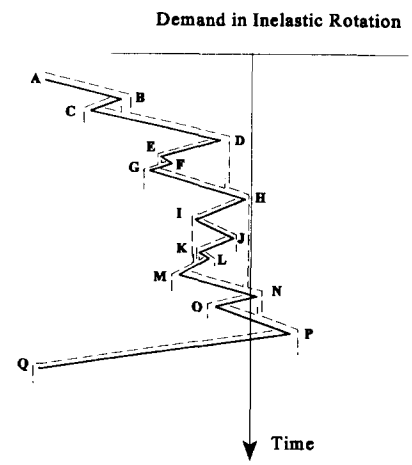

(b) Deformation history

Fig. 14 Strong motion response of a beam in a seven storey building.

a increases, while that of b is relatively stable around an average value of 1.648 (Fig. 12). In Fig. 11, section 310W21 having an effective slenderness α_e of 0.71 is shown to exhibit a noticeably greater deterioration rate than does section HE220B whose effective slenderness α_e is 0.115. Using the least squares method, parameter a was expressed in terms of the effective slenderness α_e as follows:

$$a = -1.98 + 14.3\ \alpha_e \tag{4}$$

Here, parameter b was taken as 1.648, the average value of the specimens mentioned in Table 2. In fact, in a study by Krawinkler (1987), it was suggested that unlike parameter a believed to be of a random nature, parameter b was noted to be a much more stable parameter in the range of 1.5 to 2.0. Note that good agreement is shown to exist between the observed values of the parameters a and b and those empirically predicted.

Eq. 1 along with Eq. 4 were then used to generate a comprehensive model for the prediction of strength deterioration per reversal of loading (Fig. 13). The model can be used in numerical

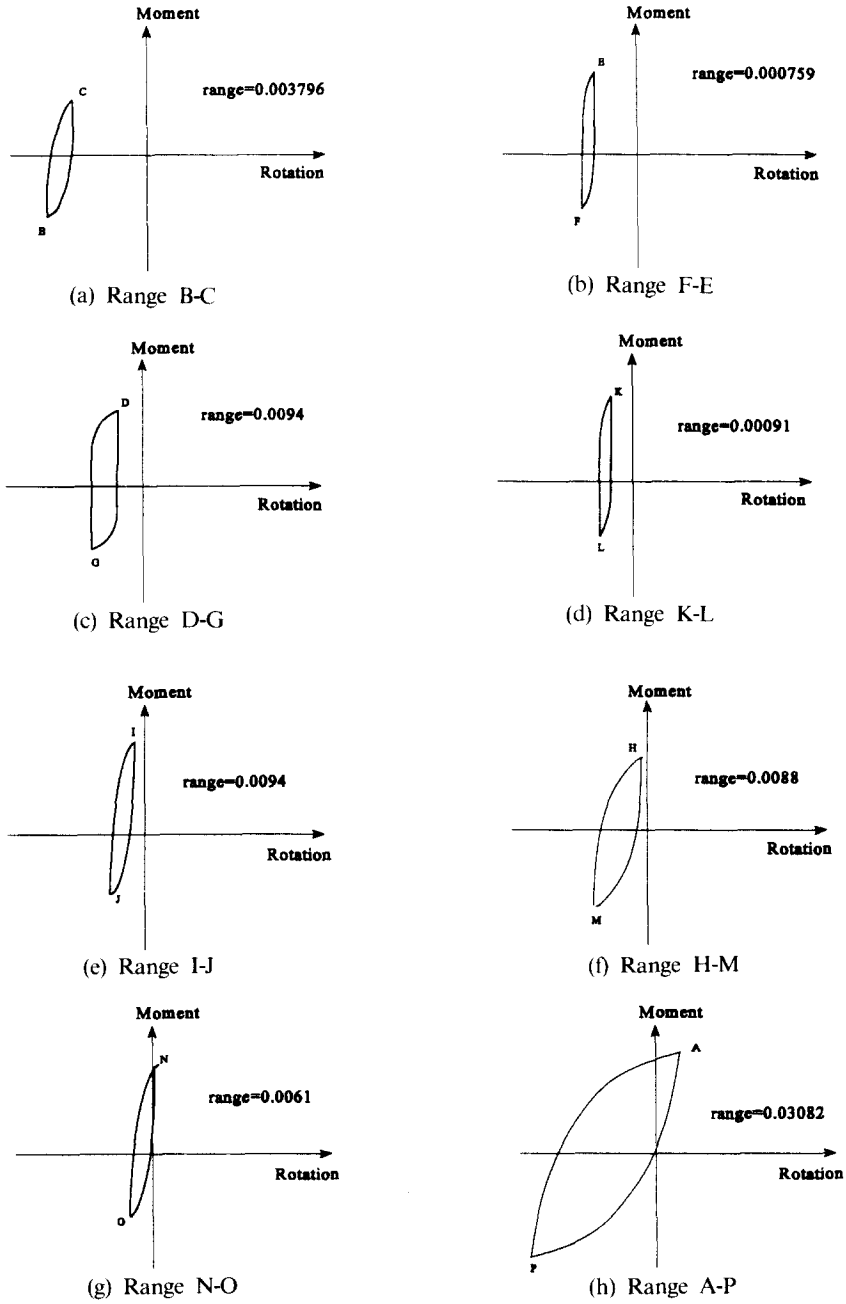

Fig. 15 Identification of closed loops using rain-flow method.

nonlinear analyses of ductile moment resisting frames along with the rain-flow cycle counting method (Downing and Socie 1982) to yield information on the level of deterioration in strength or dissipated energy sustained in a structural member during a prescribed load history. Practical implications of the model can be seen in the evaluation of damage accumulation in members belonging to Class 1 (or plastic design) sections. It should be noted however that since the method described is based on limited data, the actual expressions for determination of the para-

meters a and b may not be as accurate as a broad set of experiments could provide. Nonetheless the approach is deemed to be a reasonable way of predicting damage in steel beams under cyclic loading.

4.2.4. Example of application

Consider the inelastic rotation response of a W610×125 beam section belonging to a seven storey building subjected to a strong motion earthquake record history (Fig. 14). The beam section has the following characteristics: $\alpha_f=7.65$, $\alpha_w=54.57$ and $\alpha_l=56.58$. As such the effective slenderness α_e is 0.7854 and using Eq. 4 we obtain: $a=9.25$ with b being given the average value of 1.65.

To be able to apply the knowledge derived from the constant amplitude tests, one needs to convert the random response in an equivalently ordered response expressed in terms of closed loops of constant amplitude deformation. For that, we would apply the rain-flow method or any other applicable method found in the literature. For more details the reader is referred to Bannantine, *et al.* (1990) where an excellent summary of such methods is covered. A rain-flow algorithm written by Downing and Socie (1982) was modified by the authors and used to identify the constant amplitude deformation closed loops and their corresponding ranges. Using Eq. 3, the cumulated damage in strength deterioration is obtained as: $d=(9.25)(2)[0.003796^{1.65}+0.0007592^{1.65}+0.0094^{1.65}+\cdots]$ where the values within the square bracket are obtained from Fig. 15 and represent the plastic rotation range values.

In this example, $d=9.1\%$ of the maximum resisting force. Note that the number 2 reflects the fact that there are two reversals per complete cycle.

5. Summary and conclusions

Ductile moment resisting frames must have their beams able to both develop the plastic moment capacity and sustain an accompanying sufficient inelastic rotation. Under strong earthquake motions, structural elements may undergo a high inelastic excursion followed by a number of inelastic reversals which will eventually affect their restoring force characteristics. The experimental results of seven specimens tested under different load histories were shown to yield different rotation capacities under monotonic and cyclic loading. This, therefore, raises the question about the need for reviewing slenderness code limits when cyclic loading effects are present.

To further shed some light on the low cycle fatigue effects due to local buckling, results of three different constant amplitude tests on similar specimens were used to yield a Coffin-Manson type of equation, giving the deterioration (in strength, dissipated energy) per reversal of loading. Furthermore, Miner's rule was used to obtain the cumulated damage in the number of reversals. Finally, the experimental results of the constant amplitude tests of this study along with earlier ones were used to propose a strength damage assessment model for beams. Indeed, the model uses the plate and lateral slenderness of the beam to predict the strength deterioration per reversal of loading and the cumulated damage after N number of reversals.

In conclusion, one can say that: (a) Strength and energy deterioration appear to depend on a combined slenderness parameter that is the product of flange, web and lateral slenderness values. (b) A damage model for strength and energy deterioration has been proposed. The applicability of the damage model has been demonstrated on a beam element of a structure subjected to a strong motion earthquake. The model can prove very useful in nonlinear analysis of ductile

moment resisting frames subjected to earthquake loading by highlighting the element which may have been inadequately selected.

Notations

b	flange width
D	cumulated damage in N reversals
d	deterioration per reversal
h	clear depth of web between flanges
t	flange thickness
F_y	resisting force at yield
F_u	resisting force at ultimate
E	energy dissipated in a given one full reversal
E_u	energy dissipated in the first full reversal before a significant degradation takes place
M	beam moment
M_p	plastic moment
R_u	rotation capacity at ultimate deflection
r_y	radius of gyration about a section's weak axis
w	web thickness
α_f	modified flange slenderness
α_l	modified lateral slenderness
α_w	modified web slenderness
α_e	effective slenderness ratio
θ	end rotation
θ_p	plastic rotation range
θ_{pl}	rotation corresponding to plastic moment
Δd	rate of deterioration (in strength, stiffness, or dissipated energy)
σ_y	actual yield stress
W310×39	W-shape section with 310 mm depth, 165 mm width and 0.38 kN/m weight
W310×21	W-shape section with 303 mm depth, 101 mm width and 0.207 kN/m weight
W610×125	W-shape section with 612 mm depth, 229 mm width and 1.22 kN/m weight

References

Bannantine, J.A., *et al.* (1990), *Fundamentals of metal fatigue analysis,* Prentice Hall, Englewood Cliffs, NJ.

Castiglioni, C.A. and Goss, G. (1989), "Sulla applicabilita della regola di Miner nella fatica a basso numero di cicli", *Politecnico di Milano,* 8/89.

Castiglioni, C.A. (1992), "Assessment of seismic damage in steel members using Miner's rule", *Politecnico di Milano,* 1/92.

Castiglioni, C.A. and Losa, P.L. (1992), "Local buckling and structural damage in steel members under cyclic loads", *10 WCEE,* Rotterdam.

Calado, L. and Azevado, J. (1989), "A model for predicting the failure of structural steel elements", *J. Construct. Steel Research,* **14**.

Calado, L. (1992), "Influence of the cross-section of steel beam columns on the seismic design", *Proc. 10 WCEE,* Rotterdam.

Downing, S.D. and Socie, D.F. (1982), "Simple rain-flow counting algorithms", *Int. J. Fatigue.*

Gyoten, Y., *et al.* (1974), "Experimental study on low cycle fatigue of a structural member subjected to earthquake loads", *Proc. 5 WCEE,* **1**, Rome.

Kasiraj, I. and Yao, J.T.P. (1969), "Fatigue damage in seismic structures", *ASCE,* **95**(ST8).

Krishnasamy, S. and Sherbourne, A.N. (1968), "Response of a plastic hinge to low cycle alternating deflections", *Experimental Mechanics*, **8**(6).
Krawinkler, H. and Zohrei, M. (1983), "Cumulative damage in steel structures subjected to earthquake ground motions", *Computers and Structures*, **16**(1-4).
Krawinkler, H. (1982), "Selection of loading histories for seismic testing of structural components", *Proc. Joint Conf. on Experimental Mechanics*, Hawaii.
Krawinkler, H. (1987), "Performance assessment of steel components", *Earthquake Spectra*, **3**(1).
Mizuhata, K., *et al.*, (1977), "Study on low cycle fatigue of structural frames due to randomly varying load", *6 Proc. WCEE*, New Delhi, India.
Miner, M. A. (1945), "Cumulative damage in fatigue", *ASME*.
Neale, K. and Schroeder, J. (1971), "Instability under cycles of plastic deformations", in Leipholz, H., Ed., *Instability of Continuous Systems*, Springer-Verlag, Berlin.
Sherbourne, A.N. (1963), "Some preliminary experiments on the behaviour of ductile structures under repeated loads", *Experimental Mechanics*, **3**(5).
Tavernelli, J.F. and Coffin, L.F. (1961), "Experimental support for generalized equation predicting low cycle fatigue", *ASME*, Paper 61.
Yamada, M. (1969), "Low cycle fatigue fracture limits of various kinds of structural members subjected to alternately repeated plastic bending under axial compression as an evaluation basis or design criteria for aseismic capacity", *Proc. 4 WCEE*, Santiago de Chile.